Acta Polytechnica **62**(1):23–29, 2022
https://doi.org/10.14311/AP.2022.62.0023

Published by the Czech Technical University in Prague

PHOTONIC GRAPHENE UNDER STRAIN WITH POSITION-DEPENDENT GAIN AND LOSS

Miguel Castillo-Celeita[a,*], Alonso Contreras-Astorga[b], David J. Fernández C.[a]

[a] *Cinvestav, Physics Department, P.O. Box. 14-740, 07000 Mexico City, Mexico*

[b] *Cinvestav, CONACyT – Physics Department, P.O. Box. 14-740, 07000 Mexico City, Mexico*

[*] corresponding author: mfcastillo@fis.cinvestav.mx

Abstract. We work with photonic graphene lattices under strain with gain and loss, modeled by the Dirac equation with an imaginary mass term. To construct such Hamiltonians and their solutions, we use the free-particle Dirac equation and then a matrix approach of supersymmetric quantum mechanics to generate a new Hamiltonian with a magnetic vector potential and an imaginary position-dependent mass term. Then, we use a gauge transformation that maps our solutions to the final system, photonic graphene under strain with a position-dependent gain/loss term. We give explicit expressions for the guided modes.

Keywords: Graphene, Dirac materials, photonic graphene, matrix supersymmetric, quantum mechanics.

1. Introduction

Graphene is the last known carbon allotrope, it was isolated for the first time by Novoselov, Geim, et al. in 2004 [1]. This material consists of a two-dimensional hexagonal arrangement of carbon atoms. Graphene excels for its interesting properties, such as mechanical resistance, electrical conductivity, and optical opacity [2, 3]. The study of graphene has contributed to the development of different areas in physics, for example, in solid-state, graphene has prompted the discovery of other materials with similar characteristics, such as borophene and phosphorene. At low energy, the charge carriers in graphene behave like Dirac massless particles, and from this approach, graphene has allowed the verification of the Klein tunneling paradox as well as the quantum Hall effect. These phenomena have gained a special interest in particle physics and quantum mechanics [4].

Exploring graphene in an external constant magnetic field has allowed identifying the discrete bound states in the material, the so-called Landau levels. Moreover, theoretical physicist have analyzed the behavior of Dirac electrons in graphene under different magnetic field profiles as well. Supersymmetric quantum mechanics is a useful tool to find solutions of the Dirac equation under external magnetic fields [5–9]. Following this approach, a mechanical deformation in a graphene lattice is equivalent to introducing an external magnetic field [10, 11].

Graphene has its analog in photonics, called *photonic graphene*. It is constructed through a two-dimensional photonic crystal with weakly coupled optical fibers in a three-dimensional setting [12–17]. Photonic graphene under strain is modeled through a deformation in the coupled optical fiber lattice [18–21].

Compared with the conventional graphene Hamiltonian, the photonic graphene Hamiltonian has an extra term that represents the gain/loss in the fibers. The literature on this topic always considers a constant gain/loss in space. With the previous motivation, we will apply supersymmetric quantum mechanics in a matrix approach (matrix SUSY-QM) to obtain solutions of the Dirac equation for strain photonic graphene with a position-dependent gain/loss.

2. Strain in photonic graphene

The graphene structure consists of carbon atoms in a hexagonal arrangement similar to a honeycomb lattice. This structure can be described by two triangular sublattices of atoms, which are denoted as type A and type B. The base vectors to the unitary cell are given by

$$\mathbf{a}_1 = \frac{a}{2}(\sqrt{3}, 3), \quad \mathbf{a}_2 = \frac{a}{2}(-\sqrt{3}, 3), \tag{1}$$

where a is the interatomic distance, for graphene $a = 1.42$ Å (see Figure 1a). The position of the atoms in the whole lattice can be defined by the set of vectors $R_l = l_1\mathbf{a}_1 + l_2\mathbf{a}_2$, with $l_1,\ l_2 \in \mathbb{Z}$. An alternative description of graphene is through the first neighbors, which are connected by the vectors δ_n

$$\delta_1 = \frac{a}{2}(\sqrt{3}, 1), \quad \delta_2 = \frac{a}{2}(-\sqrt{3}, 1), \quad \delta_3 = a(0, -1). \tag{2}$$

A reciprocal lattice can be defined in the momentum space, which is also hexagonal, as shown in Figure 1b. It is rotated 90° with respect to the original carbon network. A hexagon in the reciprocal lattice is recognized as the first Brillouin zone. In this zone, there are only two inequivalent points, $\mathbf{K}_\pm = (\pm\frac{4\pi}{3\sqrt{3}a}, 0)$.

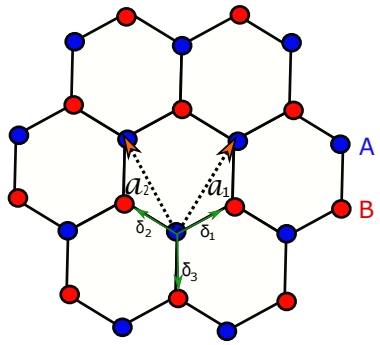

(A).

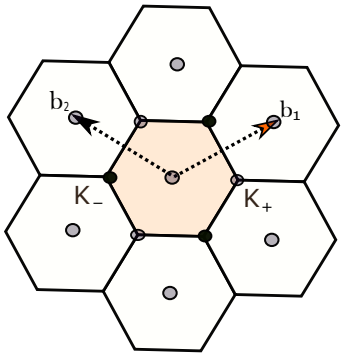

(B).

Figure 1. (A) Hexagonal graphene lattice. The lattice is constructed by type A and type B atoms, in this case, $\mathbf{a}_1$ and $\mathbf{a}_2$ correspond to the lattice unitary vectors, and δ_n are the vectors that connect the atoms A(B) with the nearest neighbors. (B) Reciprocal lattice, which is characterized by the $b_{1,2}$ vectors and $K_\pm$ correspond to the two possible inequivalent points in the lattice.

All subsequent corners are determined from either $\mathbf{K}_+$ or $\mathbf{K}_-$ plus integer multiples of the vectors

$$\mathbf{b}_1 = \frac{2\pi}{3a}(\sqrt{3}, 1), \quad \mathbf{b}_2 = \frac{2\pi}{3a}(-\sqrt{3}, 1). \tag{3}$$

Vectors $\mathbf{a}_i$ and $\mathbf{b}_j$ fulfill the condition $\mathbf{a}_i \cdot \mathbf{b}_j = 2\pi\delta_{ij}$.

2.1. Tight-binding model

The tight-binding Hamiltonian describes the hopping of an electron from an atom A (B) to an atom B (A)

$$H = -t\sum_{R_i}\sum_{n=1}^{3}(|A_{R_i}\rangle\langle B_{R_i+\delta_n}| + |B_{R_i+\delta_n}\rangle\langle A_{R_i}|), \tag{4}$$

where $t \approx$ 3 eV is called the hopping integral, R_i runs over all sites in the sublattice A, thus $|A_{R_i}\rangle$ is a state vector in these sites, the same applies to B and $|B_{R_i+\delta_n}\rangle$, recall that δ_n connects the atoms of the sublattice $A(B)$ with its nearest neighbors in the sublattice $B(A)$. The translational symmetry suggests the use of Bloch states

$$|\Psi_{Bloch}\rangle = \frac{1}{\sqrt{N_c}}\sum_{R_j}(e^{ik\cdot R_j}\psi_A(k)|A_{R_j}\rangle + e^{ik\cdot(R_j+\delta_3)}\psi_B(k)|B_{R_j+\delta_3}\rangle), \tag{5}$$

where N_c is the number of the unitary cell [22]. Then $H|\Psi\rangle = E|\Psi\rangle$ becomes a matrix problem

$$\begin{pmatrix} 0 & -t\sum_{n=1}^{3} e^{-ik\cdot\delta_n} \\ -t\sum_{n=1}^{3} e^{ik\cdot\delta_n} & 0 \end{pmatrix}\begin{pmatrix}\psi_A \\ \psi_B\end{pmatrix} = E\begin{pmatrix}\psi_A \\ \psi_B\end{pmatrix}, \tag{6}$$

with $\psi_A \equiv \psi_A(k)$ and $\psi_B \equiv \psi_B(k)$ and the energy term given by

$$E_\pm = \pm\left|t\sum_{n=1}^{3} e^{-ik\cdot\delta_n}\right| = \pm t\sqrt{3 + 2\cos(\sqrt{3}k_x a) + 4\cos(\sqrt{3}k_x\frac{a}{2})\cos(3k_y\frac{a}{2})}.$$

To obtain an effective Hamiltonian at low energy, we can consider the Taylor series around the Dirac points $H(k = \mathbf{K}_\pm + q) \approx q\cdot\nabla_k H|_{\mathbf{K}_\pm}$. Note that $E(\mathbf{K}_\pm) = 0$, as a consequence, at these points, the valence and conduction bands are connected. The above calculus leads to the analog of the Dirac-Weyl equation

$$H_\varrho\Psi = \hbar v_0(\varrho\sigma_1 q_x + \sigma_2 q_y)\Psi = E\Psi, \tag{7}$$

where $\varrho = \pm 1$ correspond to the $\mathbf{K}_\pm$ valleys, v_0 is called the Fermi velocity, in graphene, $v_0 = 3ta/2\hbar \approx c/300$, with c being the velocity of light, σ_i are the Pauli matrices

$$\sigma_1 = \begin{pmatrix}0 & 1\\ 1 & 0\end{pmatrix},\ \sigma_2 = \begin{pmatrix}0 & -i\\ i & 0\end{pmatrix},\ \sigma_3 = \begin{pmatrix}1 & 0\\ 0 & -1\end{pmatrix}, \tag{8}$$

and Ψ is a bi-spinor. The matrix nature of this equation is related to the sublattices A and B, this degree of freedom is called pseudo-spin. Notice that at low energies, the dispersion relation is linear, given by $E_\pm(q) = \pm\hbar v_0|q|$, then, the Dirac cones are connecting at $E_\pm = 0$, as expected for particles without mass [23].

2.2. Uniform strain

The photonic analog of a graphene lattice is built with weakly coupled optical fibers. This kind of photonic system is described by the same tight-binding Hamiltonian in graphene with an additional term $\gamma_{A/B}$; that represents the gain and loss in the optical fibers in the position A/B, this new term produces an attenuation or amplification in the optical modes.

If we consider uniform strain in the lattices, which is represented by a strain tensor

$$\mathbf{u} = \begin{pmatrix}\mathbf{u}_{11} & 0\\ 0 & \mathbf{u}_{22}\end{pmatrix}, \tag{9}$$

the Fermi velocity is modified in the following form

$$\mathbf{v}_{ij} = v_0(1 + (1-\beta)\mathbf{u}_{ij}). \tag{10}$$

The hopping integrals are modified with a little perturbation $t \to t_n$, that, considering the changes in the orbitals by the modification of the carbon distances

$$t_n \approx t\left(1 - \frac{\beta}{a^2}\delta_n\cdot\mathbf{u}\cdot\delta_n\right), \tag{11}$$

where

$$\beta = -\frac{\partial \ln t}{\partial \ln a} \tag{12}$$

is the Grüneisen parameter that depends on the model; for graphene, β is between 2 and 3 [10] (see also [24, 25]). In photonic graphene, a is the distance between adjacent waveguides. The Hamiltonian of a photonic graphene with a uniform strain reads as

$$H = \gamma_A \sum_{R_i} |A_{R_i}\rangle \langle A_{R_i}| + \gamma_B \sum_{R_i} |B_{R_i+\delta_n}\rangle \langle B_{R_i+\delta_n}| - \sum_{R_i}\sum_{n=1}^{3} t_n (|A_{R_i}\rangle \langle B_{R_i+\delta_n}| + |B_{R_i+\delta_n}\rangle \langle A_{R_i}|). \tag{13}$$

The deformation of the lattice produces a shift of the Dirac points $\mathbf{K}_\pm^D \approx (\mathbf{1}-\mathbf{u})\cdot\mathbf{K}_\pm \pm \mathbf{A}$, where $\mathbf{A} = (\mathbf{A}_x, \mathbf{A}_y)$

$$\mathbf{A}_x = \frac{\beta}{2a}(\mathbf{u}_{11} - \mathbf{u}_{22}), \quad \mathbf{A}_y = -\frac{\beta}{2a}(2\mathbf{u}_{12}). \tag{14}$$

Using the Bloch solution, the Hamiltonian under strain takes the form:

$$H = \begin{pmatrix} \gamma_A & -\sum_{n=1}^{3} t_n e^{-ik\cdot(\mathbf{1}-\mathbf{u})\cdot\delta_n} \\ -\sum_{n=1}^{3} t_n e^{ik\cdot(\mathbf{1}-\mathbf{u})\cdot\delta_n} & \gamma_B \end{pmatrix}, \tag{15}$$

under the assumption $|\mathbf{u}\cdot\delta_n| \ll a$. In this work, we will assume that $\gamma_A = i\gamma$ and $\gamma_B = \gamma_A^*$, then, for positive γ, the waveguides in the sublattice A (B) present the energy gain (loss), as in the arrangements proposed in [14]. Expanding this Hamiltonian around the Dirac points, through the substitution $k = \mathbf{K}_\pm^D + q$, one arrives at a Dirac Hamiltonian analog with minimal coupling

$$H = v_0\sigma\cdot(\mathbf{1} + \mathbf{u} - \beta\mathbf{u})q + i\gamma\sigma_3. \tag{16}$$

Comparing with (7), the effect of strain is equivalent, to consider magnetic-like field modeled through a pseudo-magnetic vector potential $\mathbf{A}$. The last term represents a gain/loss balance in sublattices A/B. In photonic graphene, strain could be generated by deformations in the geometry of the optical-fiber lattice.

2.3. Non-uniform strain

For non-uniform strain, the deformation matrix depends of the position, $\mathbf{u} \to \mathbf{u}(r)$. Thus, the expression for the Hamiltonian becomes

$$H = -i\sigma_i\sqrt{\mathbf{v}_{ij}}\partial_j\sqrt{\mathbf{v}_{ij}} + v_0\sigma_i\mathbf{A}_i + i\gamma\sigma_3, \tag{17}$$

considering a strain tensor of the form

$$\mathbf{u} = \begin{pmatrix} \mathbf{u}_{11}(x) & 0 \\ 0 & \mathbf{u}_{22}(y) \end{pmatrix}, \tag{18}$$

and equations (10) and (14), still apply. We can also write the strain Hamiltonian as

$$H(x,y) = -i\sigma_1\sqrt{\mathbf{v}_{11}}\partial_x\sqrt{\mathbf{v}_{11}} - i\sigma_2\sqrt{\mathbf{v}_{22}}\partial_y\sqrt{\mathbf{v}_{22}} + \sigma_1\frac{v_0\beta}{2a}(\mathbf{u}_{11}(x) - \mathbf{u}_{22}(y)) + i\gamma\sigma_3, \tag{19}$$

where $\mathbf{v}_{11} = \mathbf{v}_{11}(x)$, $\mathbf{v}_{22} = \mathbf{v}_{22}(y)$.

We can relate the eigenvalue equation of this Hamiltonian, $H\Psi = E\Psi$, with a strain-free one using the following transformation. First, we define the coordinates

$$r = \int \frac{v_0}{\mathbf{v}_{11}(x)}dx, \quad s = \int \frac{v_0}{\mathbf{v}_{22}(y)}dy, \tag{20}$$

and the operator

$$G(x,y) = \frac{\sqrt{\mathbf{v}_{11}\mathbf{v}_{22}}}{v_0}\exp\left(\frac{iv_0\beta}{2a}\int_0^x \frac{\mathbf{u}_{11}(q)}{\mathbf{v}_{11}(q)}dq\right), \tag{21}$$

then, H will be related with a flat Fermi velocity Hamiltonian H_0 as

$$H(x,y) = G^{-1}(x,y)H_0(r(x),s(y))G(x,y), \tag{22}$$

where

$$H_0\Phi = \left(-iv_0\sigma_1\partial_r - iv_0\sigma_2\partial_s - \frac{v_0\beta}{2a}\mathbf{u}_{22} + i\gamma\sigma_3\right)\Phi, \tag{23}$$

and $\mathbf{u}_{22} = \mathbf{u}_{22}(y(r,s))$. The solutions are mapped as

$$\Psi(x,y) = G^{-1}(x,y)\Phi(r(x),s(y)). \tag{24}$$

The energy spectrum is the same for both Hamiltonians [18, 19, 26].

3. Supersymmetric quantum mechanics: matrix approach

Supersymmetric quantum mechanics (SUSY-QM) is a method that relates two Schrödinger Hamiltonians through an intertwining operator [27, 28]. Another approach is the matrix SUSY-QM, which intertwines two Dirac Hamiltonians H_0, H_1 by a matrix operator L. In this work, we use the latter to construct an appropriate Hamiltonian H_1 that will be linked via the operator G introduced in (21) to a photonic graphene system under strain. For the sake of completeness we will give a brief review of matrix SUSY-QM (more details can be found in [29]).

We start by proposing the following intertwining relation:

$$L_1H_0 = H_1L_1, \tag{25}$$

where the Dirac Hamiltonians are given by

$$H_0 = -i\sigma_2\partial_s + V_0(s), \quad H_1 = -i\sigma_2\partial_s + V_1(s), \tag{26}$$

and the intertwining operator is

$$L_1 = \partial_s - U_sU^{-1}, \tag{27}$$

with U being a matrix function called *seed* or *transformation matrix*, the subindex in U_s represent the derivative respect to s, and U must satisfy $H_0U = U\Lambda$. Let us write U in a general form and Λ as a diagonal matrix

$$U = \begin{pmatrix} u_{11} & u_{12} \\ u_{21} & u_{22} \end{pmatrix}, \quad \Lambda = \begin{pmatrix} \lambda_1 & 0 \\ 0 & \lambda_2 \end{pmatrix}. \tag{28}$$

From the intertwining relation and the given definitions, the potential V_1 can be written in terms of the potential V_0 and the transformation matrix as

$$V_1 = V_0 + i[U_s U^{-1}, \sigma_2]. \tag{29}$$

Solutions of the Dirac equation $H_0\xi = E\xi$ can be mapped onto solutions of $H_1\Phi = E\Phi$ using the intertwining operator as $\Phi \propto L_1\xi$. There are some extra solutions, usually referred to *missing states*. They can be obtained from each column of $(U^T)^{-1}$, named Φ_{λ_j}, $j = 1, 2$, which satisfy $H_1\Phi_{\lambda_j} = \lambda_j\Phi_{\lambda_j}$. If the vectors Φ_{λ_j} fulfill the boundary conditions of the problem, λ_j must be included in the spectrum of H_1. As a summary, with this technique, we start from H_0, its eigenspinors and spectrum, then we construct H_1, obtain the solutions of the corresponding Dirac equation and the spectrum. Now, let us mention that it is possible to iterate this technique. The main advantage comes from the modification of the spectrum, since with each iteration, we can add more energy levels. The second-order matrix SUSY-QM can be reached through a second intertwining relation

$$L_2 H_1 = H_2 L_2, \tag{30}$$

which is similar to (25). The intertwining operator now takes the form

$$L_2 = \partial_s - (\mathcal{U}_2)_s \mathcal{U}_2^{-1}. \tag{31}$$

The operator L_1 is used to determine the transformation matrix of the second iteration, $\mathcal{U}_2 = L_1 U_2$, where U_2 fulfills the relation $H_0 U_2 = U_2 \Lambda_2$. In this case, Λ_2 is an Hermitian matrix that we choose diagonal once again,

$$\Lambda_2 = \begin{pmatrix} \widetilde{\lambda}_1 & 0 \\ 0 & \widetilde{\lambda}_2 \end{pmatrix}, \quad U_2 = \begin{pmatrix} w_{11} & w_{12} \\ w_{21} & w_{22} \end{pmatrix}. \tag{32}$$

The elements of Λ_2 are such that $(\widetilde{\lambda}_1, \widetilde{\lambda}_2) \neq (\lambda_1, \lambda_2)$. Therefore, the second order potential is given by

$$V_2 = V_1 + i\left[(\mathcal{U}_2)_s \mathcal{U}_2^{-1}, \sigma_2\right]. \tag{33}$$

The solutions of $H_2\chi = E\chi$ are obtained from the eigenspinors of H_1 as $\chi \propto L_2\Phi$. The second-order matrix SUSY-QM generates, in principle, two sets of eigenspinors that correspond to the columns of the matrices $(\mathcal{U}_2^T)^{-1}$ and $L_2(U^T)^{-1}$.

4. Photonic graphene under strain and position-dependent gain and loss

In this section, we start from the auxiliary Dirac equation of a free particle with imaginary mass, and using a matrix SUSY-QM and a gauge transformation G, we obtain a photonic graphene model with strain and position dependent gain/loss. We show that we can iterate the technique to add more propagations modes.

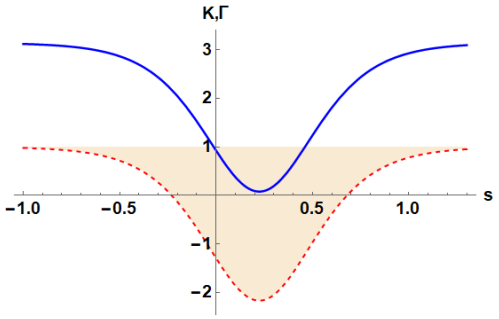

Figure 2. Graph of the functions $v_0k_r + K(s)$ (line blue) and the gain/loss term $\gamma - \Gamma(s)$ (dashed red line) for $\epsilon = 1.5$, $k_r = \pi$, $\gamma = 1$, $v_0 = 1.0$. Notice that $\gamma - \Gamma(s)$ coincides asymptotically with γ.

4.1. Photonic Graphene with a single mode

Let us start from the free particle Dirac equation where we included a purely imaginary mass term:

$$H_0\Phi = (-iv_0\sigma_1\partial_r - iv_0\sigma_2\partial_s + i\gamma\sigma_3)\Phi. \tag{34}$$

Considering $\Phi(r, s) = \exp(ik_r r)(\phi_A(s), \phi_B(s))^T$, the Hamiltonian can be written as

$$H_0(r, s) = -iv_0\sigma_2\partial_s + V_0, \tag{35}$$

where $V_0 = v_0k_r\sigma_1 + i\gamma\sigma_3$. Now, we use the matrix SUSY-QM to construct a new system. A convenient selection of the Λ elements is $\lambda_1 = \epsilon = -\lambda_2$. We build the transformation matrix U with the entries $u_{21} = u_{22}^* = \cosh(\kappa s) + i\sinh(\kappa s)$, the corresponding momentum in s is given by $\kappa = \sqrt{k_r^2 - (\gamma^2 + \epsilon^2)/v_0^2}$. The other two components are found through the equation:

$$u_{1j} = \frac{v_0}{(\lambda_j - i\gamma)}(-u'_{2j} + k_r u_{2j}), \quad j = 1, 2. \tag{36}$$

From (29) we obtain V_1 as

$$V_1 = V_0 + \sigma_1 K(s) - i\sigma_3\Gamma(s), \tag{37}$$

where $\Gamma(s)$, $K(s)$ are given by

$$\Gamma = 2\gamma + \frac{2\epsilon\left(\kappa(\gamma\sinh(2\kappa s) + \epsilon) - \gamma k_r\cosh(2\kappa s)\right)}{\kappa(\gamma - \epsilon\sinh(2\kappa s)) + k_r\epsilon\cosh(2\kappa s)},$$

$$K = \frac{2v_0k_r\epsilon\left(k_r\cosh(2\kappa s) - \kappa\sinh(2\kappa s)\right)}{\kappa(\gamma - \epsilon\sinh(2\kappa s)) + k_r\epsilon\cosh(2\kappa s)} - 2v_0k_r.$$

Figure 2 shows a plot of the functions $v_0k_r + K(s)$ and $\gamma - \Gamma(s)$. The new Hamiltonian takes the form

$$H_1(r, s) = -i\sigma_2v_0\partial_s + \sigma_1(-iv_0\partial_r + K) + i\sigma_3(\gamma - \Gamma). \tag{38}$$

This system supports two single bound states. They are the columns of the matrix $(U^T)^{-1} = (\Phi_\epsilon, \Phi_{-\epsilon})$. The eigenvector associated with ϵ is given by

$$\Phi_\epsilon(r, s) = \frac{e^{ik_r r}}{2}\begin{pmatrix} -\frac{(\gamma^2+\epsilon^2)(\cosh(\kappa s)+i\sinh(\kappa s))}{v_0\kappa(\gamma-\epsilon\sinh(2\kappa s))+v_0k_r\epsilon\cosh(2\kappa s)} \\ \frac{(\gamma-i\epsilon)((\kappa+ik_r)\cosh(\kappa s)-(k_r+i\kappa)\sinh(\kappa s))}{\kappa(\gamma-\epsilon\sinh(2\kappa s))+k_r\epsilon\cosh(2\kappa s)} \end{pmatrix}. \tag{39}$$

Our next step is to apply the gauge transformation defined in (20)-(22). The strain and Fermi velocity tensors that we consider are

$$\mathbf{u} = \begin{pmatrix} 0 & 0 \\ 0 & -\frac{2aK(y))}{\beta} \end{pmatrix},$$
$$\mathbf{v} = v_0 \begin{pmatrix} 1 & 1 \\ 1 & 1-(1-\beta)\frac{2aK(y)}{\beta} \end{pmatrix}, \qquad (40)$$

see (18). The change of variables in (20) becomes

$$r = x, \quad s = \int \frac{1}{1-(1-\beta)\frac{2aK(y)}{\beta}} dy, \qquad (41)$$

and the operator $G(x,y) = \sqrt{1-(1-\beta)\frac{2aK(y)}{\beta}}$. This choice leads to the following Hamiltonian

$$H_1(x,y) = -iv_0\sigma_1\partial_x - i\sigma_2\sqrt{\mathbf{v}_{22}(y)}\partial_y\sqrt{\mathbf{v}_{22}(y)} - \sigma_1\frac{v_0\beta}{2a}\mathbf{u}_{22}(y) + i(\gamma-\Gamma(y))\sigma_3. \qquad (42)$$

Bounded eigenstates of H_1 can be found as $\Psi_\epsilon(x,y) = G^{-1}(x,y)\Phi_\epsilon(r(x),s(y))$. In this system, there is a single mode in the upper Dirac cone and another in the bottom cone.

The strain generates an analog of a magnetic field perpendicular to the graphene layer $\vec{\mathbf{B}}(y) = (\beta/2a)\partial_y\mathbf{u}_{22}\hat{z}$. Since we are working with a photonic graphene, such a pseudo-magnetic field affects light. Moreover, the term $i\Gamma(y)\sigma_3$ indicates a position dependent gain/loss in the optical fibers of the sublattice A/B. Figure 3a shows the square modulus of each component of $\Phi_\epsilon = (\phi_{\epsilon A}, \phi_{\epsilon B})^T$ (shadowed curves) and the intensity $|\phi_{\epsilon A}|^2 + |\phi_{\epsilon B}|^2$ (red curve). Figure 3b shows the same for the mode Ψ_ϵ.

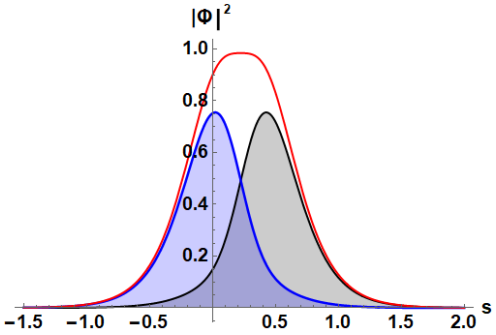

(A).

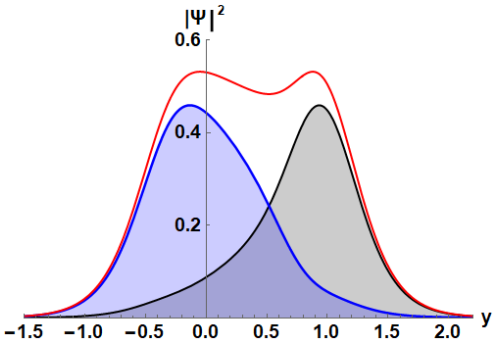

(B).

FIGURE 3. (A) Plot of the individual intensities $|\phi_{\epsilon A}|^2$ (gray curve) and $|\phi_{\epsilon B}|^2$ (blue curve) and the total intensity $|\phi_{\epsilon A}|^2 + |\phi_{\epsilon B}|^2$ (red line). (B) Analog of the (A) plot for the solution Ψ_ϵ of the Hamiltonian under strain. The parameters in this case are: $k_r = \pi$, $\epsilon = 1.5$, $a = 1.0$, $\beta = 0.8$, $\gamma = 1$, $v_0 = 1.0$.

4.2. Photonic Graphene with two modes

In this subsection, we use two iterations of the matrix SUSY-QM, starting again from the free-particle Hamiltonian. Let us choose an initial system with zero gain/loss ($\gamma = 0$), which is a massless fermion in graphene. In the first matrix SUSY-QM step we use the same transformation matrix U as in the example above. The first matrix SUSY-QM partner Hamiltonian has the form

$$H_1 = -i\sigma_2 v_0\partial_s + \sigma_1 K(s) + i\sigma_3\Gamma(s), \qquad (43)$$

where $K(s) = k_r v_0$,

$$\Gamma(s) = \frac{2\epsilon v_0\kappa}{\kappa v_0\sinh(2\kappa s) - k_r v_0\cosh(2\kappa s)}, \qquad (44)$$

with $\kappa = \sqrt{(k_r v_0)^2 - \epsilon^2}/v_0$. As a result of the first matrix SUSY-QM step, it is generated a position dependent gain/loss term $\Gamma(s)$. The iteration of the method requires to define the second diagonal matrix Λ_2, with $\widetilde{\lambda}_1 = -\widetilde{\lambda}_2 = \epsilon_1 \neq \epsilon$, and the second transformation matrix U_2. For this example, we

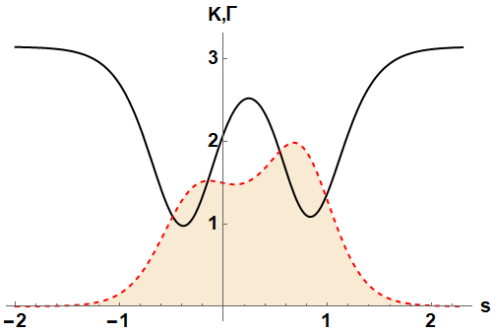

FIGURE 4. Graph of the function $v_0k_r + K_2(s)$ (black line), and the gain/loss function $\Gamma(s) + \Gamma_2(s)$ (red dashed line), for $\epsilon = 1.5$, $\epsilon_1 = 2.0$, $k_r = \pi$, $\gamma = 0$, $v_0 = 1.0$.

choose $w_{21} = \cosh(\kappa_2 s)$ and $w_{22} = \cosh(\kappa_2 s)$, where $\kappa_2 = \sqrt{(k_r v_0)^2 - \epsilon_1^2}/v_0$. The other two components can be found through the equation

$$w_{1j} = \frac{v_0}{\widetilde{\lambda}_j}(-w'_{2j} + k_r w_{2j}), \quad j = 1, 2. \qquad (45)$$

The potential V_2 can be calculated from (33), $V_2 = V_1 + \sigma_1 K_2(s) + i\sigma_3\Gamma_2(s) = V_0 + \sigma_1 K_2 + i\sigma_3(\Gamma + \Gamma_2)$. The functions $v_0k_r + K_2(s)$ and $\Gamma(s) + \Gamma_2(s)$ are shown in Figure 4. It is important to highlight that the gain/loss term remains a pure imaginary quantity.

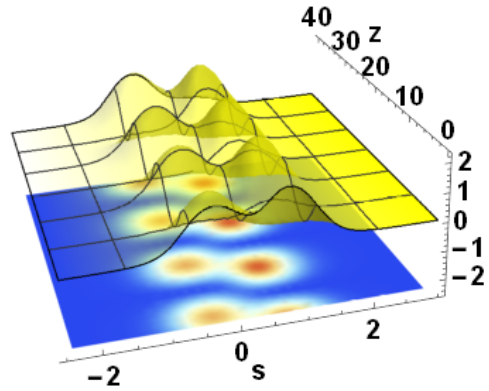

(A).

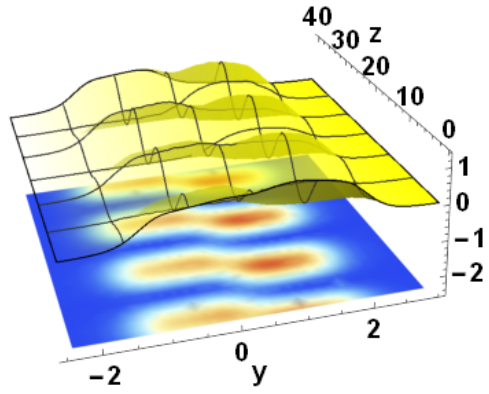

(B).

Figure 5. (A) Intensity of the superposition $|\bar{\Phi}(s,z)|^2$ propagating in the z-axis. (B) Intensity of the superposition $|\bar{\Psi}(y,z)|^2$. The values of the parameters taken are $\epsilon = 1.5$, $\epsilon_1 = 2.0$, $k_r = \pi$, $\gamma = 0$, $\beta = 0.8$, $a = 1.0$, $v_0 = 1.0$.

The second matrix SUSY-QM step introduces two new sets of eigenmodes. They can be extracted from the columns of the matrix $(\mathcal{U}_2^T)^{-1} = (\chi_{\epsilon_1}, \chi_{-\epsilon_1})$. The eigenmodes added in the first step are mapped as $\chi_{\pm\epsilon} = L_2\Phi_{\pm\epsilon}$. Similar to the previous example, it is possible to perform the gauge transformation (20)-(22). Then, in the system under strain, the modes become

$$\Psi_{\pm\epsilon_1}(x,y) = G^{-1}(x,y)\chi_{\pm\epsilon_1}(r(x),s(y)),$$
$$\Psi_{\pm\epsilon}(x,y) = G^{-1}(x,y)\chi_{\pm\epsilon}(r(x),s(y)).$$

Therefore, in this new optical system, two guided modes are created in the upper Dirac cone and two more in the bottom Dirac cone. Finally, let us mention that we can have superpositions of the introduced modes and let them propagate along the z-axis inside the photonic graphene. For example, in the flat Fermi velocity system (before the gauge transformation),

$$\bar{\Phi}(s,z) = A_1 e^{-i\epsilon z}\Phi_\epsilon(s) + A_2 e^{-i\epsilon_1 z}\Phi_{\epsilon_1}(s), \qquad (46)$$

becomes

$$\bar{\Psi}(y,z) = A_1 e^{-i\epsilon z}\Psi_\epsilon(y) + A_2 e^{-i\epsilon_1 z}\Psi_{\epsilon_1}(y), \qquad (47)$$

in the photonic graphene system under strain with the position dependent gain/loss balance. Figure 5a shows the propagation along z-axis of the intensity $|\bar{\Phi}(s,z)|^2$, while Figure 5b shows $|\bar{\Psi}(s,z)|^2$.

5. Summary

This article shows a natural way to construct Hamiltonians associated with a photonic graphene under strain with a position-dependent gain/loss balance. The main tools that we use are a matrix approach to supersymmetric quantum mechanics and a gauge transformation. With a correct choice of a transformation matrix U, it is possible to add a bound state to the free-particle Hamiltonian using the matrix SUSY-QM, but the Dirac equation will have two new terms in the potential, $V_1 = V_0 + \sigma_1 K(s) - i\sigma_3\Gamma(s)$. The function K could be associated with a magnetic vector potential, but the function $i\Gamma$ is related to an imaginary mass term, which is difficult to interpret or realize in a solid-state graphene. The gauge transformation G maps solutions from the flat Fermi velocity system of the previous step to a graphene system under strain. At this point, it becomes relevant to work with the photonic graphene. The magnetic vector potential translates into deformations of the lattice of optical fibers, while the $i\Gamma$ function indicates the gain/loss of the fibers in the sublattice A/B. We end with the Hamiltonian of photonic graphene with a single mode. This mode is confined by the strain and the position-dependent gain/loss balance. Finally, we show that the technique can be iterated, to have two or more modes in the photonic graphene.

Acknowledgements

The authors acknowledge the support of Conacyt, grant FORDECYT-PRONACES/61533/2020. M. C-C. acknowledges as well the Conacyt fellowship 301117.

References

[1] K. S. Novoselov, A. K. Geim, S. V. Morozov, et al. Electric field effect in atomically thin carbon films. *Science* **306**(5696):666–669, 2004. https://doi.org/10.1126/science.1102896.

[2] R. C. Andrew, R. E. Mapasha, A. M. Ukpong, N. Chetty. Mechanical properties of graphene and boronitrene. *Physical Review B* **85**(12):125428, 2012. https://doi.org/10.1103/PhysRevB.85.125428.

[3] S.-E. Zhu, S. Yuan, G. C. A. M. Janssen. Optical transmittance of multilayer graphene. *EPL (Europhysics Letters)* **108**(1):17007, 2014. https://doi.org/10.1209/0295-5075/108/17007.

[4] A. K. Geim, K. S. Novoselov. The rise of graphene. In *Nanoscience and technology: a collection of reviews from nature journals*, pp. 11–19. 2009. https://doi.org/10.1142/9789814287005_0002.

[5] Ş. Kuru, J. Negro, L. M. Nieto. Exact analytic solutions for a Dirac electron moving in graphene under magnetic fields. *Journal of Physics: Condensed Matter* **21**(45):455305, 2009. https://doi.org/10.1088/0953-8984/21/45/455305.

[6] B. Midya, D. J. Fernández C. Dirac electron in graphene under supersymmetry generated magnetic fields. *Journal of Physics A: Mathematical and Theoretical* **47**(28):285302, 2014. https://doi.org/10.1088/1751-8113/47/28/285302.

[7] A. Contreras-Astorga, A. Schulze-Halberg. The confluent supersymmetry algorithm for Dirac equations with pseudoscalar potentials. *Journal of Mathematical Physics* **55**(10):103506, 2014. https://doi.org/10.1063/1.4898184.

[8] M. Castillo-Celeita, D. J. Fernández C. Dirac electron in graphene with magnetic fields arising from first-order intertwining operators. *Journal of Physics A: Mathematical and Theoretical* **53**(3):035302, 2020. https://doi.org/10.1088/1751-8121/ab3f40.

[9] A. Contreras-Astorga, F. Correa, V. Jakubský. Super-Klein tunneling of Dirac fermions through electrostatic gratings in graphene. *Physical Review B* **102**(11):115429, 2020. https://doi.org/10.1103/PhysRevB.102.115429.

[10] G. G. Naumis, S. Barraza-Lopez, M. Oliva-Leyva, H. Terrones. Electronic and optical properties of strained graphene and other strained 2D materials: a review. *Reports on Progress in Physics* **80**(9):096501, 2017. https://doi.org/10.1088/1361-6633/aa74ef.

[11] M. Oliva-Leyva, C. Wang. Theory for strained graphene beyond the Cauchy–Born rule. *Physica Status Solidi (RRL)–Rapid Research Letters* **12**(9):1800237, 2018. https://doi.org/10.1002/pssr.201800237.

[12] M. Polini, F. Guinea, M. Lewenstein, et al. Artificial honeycomb lattices for electrons, atoms and photons. *Nature Nanotechnology* **8**(9):625–633, 2013. https://doi.org/10.1038/nnano.2013.161.

[13] Y. Plotnik, M. C. Rechtsman, D. Song, et al. Observation of unconventional edge states in 'photonic graphene'. *Nature Materials* **13**(1):57–62, 2014. https://doi.org/10.1038/nmat3783.

[14] H. Ramezani, T. Kottos, V. Kovanis, D. N. Christodoulides. Exceptional-point dynamics in photonic honeycomb lattices with $\mathcal{PT}$ symmetry. *Physical Review A* **85**(1):013818, 2012. https://doi.org/10.1103/PhysRevA.85.013818.

[15] G. G. Pyrialakos, N. S. Nye, N. V. Kantartzis, D. N. Christodoulides. Emergence of type-II Dirac points in graphynelike photonic lattices. *Physical Review Letters* **119**(11):113901, 2017. https://doi.org/10.1103/PhysRevLett.119.113901.

[16] S. Grosche, A. Szameit, M. Ornigotti. Spatial Goos-Hänchen shift in photonic graphene. *Physical Review A* **94**(6):063831, 2016. https://doi.org/10.1103/PhysRevA.94.063831.

[17] T. Ozawa, A. Amo, J. Bloch, I. Carusotto. Klein tunneling in driven-dissipative photonic graphene. *Physical Review A* **96**(1):013813, 2017. https://doi.org/10.1103/PhysRevA.96.013813.

[18] A. Szameit, M. C. Rechtsman, O. Bahat-Treidel, M. Segev. $\mathcal{PT}$-symmetry in honeycomb photonic lattices. *Physical Review A* **84**(2):021806, 2011. https://doi.org/10.1103/PhysRevA.84.021806.

[19] H. Schomerus, N. Y. Halpern. Parity anomaly and Landau-level lasing in strained photonic honeycomb lattices. *Physical Review Letters* **110**(1):013903, 2013. https://doi.org/10.1103/PhysRevLett.110.013903.

[20] M. C. Rechtsman, J. M. Zeuner, A. Tünnermann, et al. Strain-induced pseudomagnetic field and photonic Landau levels in dielectric structures. *Nature Photonics* **7**(2):153–158, 2013. https://doi.org/10.1038/nphoton.2012.302.

[21] D. A. Gradinar, M. Mucha-Kruczyński, H. Schomerus, V. I. Fal'ko. Transport signatures of pseudomagnetic Landau levels in strained graphene ribbons. *Physical Review Letters* **110**(26):266801, 2013. https://doi.org/10.1103/PhysRevLett.110.266801.

[22] C. Bena, G. Montambaux. Remarks on the tight-binding model of graphene. *New Journal of Physics* **11**(9):095003, 2009. https://doi.org/10.1088/1367-2630/11/9/095003.

[23] P. Dietl, F. Piéchon, G. Montambaux. New magnetic field dependence of Landau levels in a graphenelike structure. *Physical Review Letters* **100**(23):236405, 2008. https://doi.org/10.1103/PhysRevLett.100.236405.

[24] T. M. G. Mohiuddin, A. Lombardo, R. R. Nair, et al. Uniaxial strain in graphene by Raman spectroscopy: G peak splitting, Grüneisen parameters, and sample orientation. *Physical Review B* **79**(20):205433, 2009. https://doi.org/10.1103/PhysRevB.79.205433.

[25] F. Ding, H. Ji, Y. Chen, et al. Stretchable graphene: a close look at fundamental parameters through biaxial straining. *Nano Letters* **10**(9):3453–3458, 2010. https://doi.org/10.1021/nl101533x.

[26] A. Contreras-Astorga, V. Jakubskỳ, A. Raya. On the propagation of Dirac fermions in graphene with strain-induced inhomogeneous Fermi velocity. *Journal of Physics: Condensed Matter* **32**(29):295301, 2020. https://doi.org/10.1088/1361-648X/ab7e5b.

[27] D. J. Fernández C. SUSY quantum mechanics. *International Journal of Modern Physics A* **12**(01):171–176, 1997. https://doi.org/10.1142/S0217751X97000232.

[28] D. J. Fernández C., N. Fernández-García. Higher-order supersymmetric quantum mechanics. *AIP Conference Proceedings* **744**(1):236–273, 2004. https://doi.org/10.1063/1.1853203.

[29] L. M. Nieto, A. A. Pecheritsin, B. F. Samsonov. Intertwining technique for the one-dimensional stationary Dirac equation. *Annals of Physics* **305**(2):151–189, 2003. https://doi.org/10.1016/S0003-4916(03)00071-X.